



HAL
open science

A quantitative and mechanistic model for the coupling between chemistry and clay hydration

Nicolas C.M. Marty, Sylvain Grangeon, Arnault Lassin, Benoît Made, Philippe Blanc, Bruno Lanson

► **To cite this version:**

Nicolas C.M. Marty, Sylvain Grangeon, Arnault Lassin, Benoît Made, Philippe Blanc, et al.. A quantitative and mechanistic model for the coupling between chemistry and clay hydration. *Geochimica et Cosmochimica Acta*, 2020, pp.124-135. 10.1016/j.gca.2020.05.029 . insu-03022627

HAL Id: insu-03022627

<https://insu.hal.science/insu-03022627>

Submitted on 24 Nov 2020

HAL is a multi-disciplinary open access archive for the deposit and dissemination of scientific research documents, whether they are published or not. The documents may come from teaching and research institutions in France or abroad, or from public or private research centers.

L'archive ouverte pluridisciplinaire **HAL**, est destinée au dépôt et à la diffusion de documents scientifiques de niveau recherche, publiés ou non, émanant des établissements d'enseignement et de recherche français ou étrangers, des laboratoires publics ou privés.

A quantitative and mechanistic model for the coupling between chemistry and clay hydration

Nicolas C.M. Marty^{1,*}, Sylvain Grangeon¹, Arnault Lassin¹, Benoit Madé², Philippe Blanc¹,

Bruno Lanson³

¹ BRGM, 3 Avenue Guillemin, Orléans Cedex 2, 45060, France

² Andra, 1/7 Rue Jean Monnet, 92298 Châtenay-Malabry, France

³ Univ. Grenoble Alpes, CNRS, Univ. Savoie Mont Blanc, IRD, Univ. Gustave Eiffel, ISTerre,
F-38000 Grenoble, France

* Corresponding author: n.marty@brgm.fr

Highlights

- smectite water vapor isotherms modelled using an ion exchange formalism
- model accounting for the interlayer composition and relative humidity
- model accounting for the charge location
- hydration and stability of the clay layer processed independently

Abstract

It is proposed here to describe smectite water vapor desorption isotherms using an exchange formalism that quantitatively accounts for the different hydration states and thus different water

22 contents. This approach makes it possible to reproduce both desorption isotherms and relative
23 proportions of the different hydration states as determined by X-ray diffraction. The method is
24 numerically robust and easy to implement in most reactive transport codes. The formalism is
25 satisfactory from a phenomenological point of view and accounts for the influence of external
26 parameters such as interlayer cation composition and solution cation composition and salinity
27 on clay hydration. Furthermore, in contrast to most solid solution models, this approach
28 focuses on the clay reactivity according to the charge and type of interlayer cation rather than
29 on its solubility and therefore does not require the overall thermodynamic properties of the
30 clay. In addition, such an explicit distinction of the hydration/cation exchange processes from
31 the thermodynamic stability of smectite 2:1 layer allows the use of kinetics driving slow
32 dissolution/precipitation rates if the number of exchange sites is related to the amount of clay
33 minerals.

34

35 **Keywords**

36 Clay composition, ionic strength, hydration model, exchange reaction, Gapon, Rothmund-
37 Kornfeld

38

39 **Introduction**

40 The crystal structure of clay minerals can be described as the parallel stacking of layers
41 separated from each other by an interlayer space. Smectite, a generic name that encompasses
42 several minerals (Guggenheim et al., 2006), is one of the most abundant type of clay minerals
43 in various natural settings, including soils and sediments (Griffin et al., 1968; Jackson, 1957;
44 Murray and Leininger, 1955), together with illite and chlorite. The general layer structure of
45 smectite can be described as two tetrahedral sheets sandwiching an octahedral sheet. In the
46 octahedral sheet, cations can be mainly divalent (trioctahedral smectite) or trivalent

47 (dioctahedral smectite). The isomorphic substitution of a cation by another of lower valence
48 (e.g. Al^{3+} for Si^{4+} in the tetrahedral sheet, Mg^{2+} for Al^{3+} or Li^+ for Mg^{2+} in the octahedral sheet)
49 gives rise to a permanent layer charge that is compensated for by the presence of hydrated
50 cations in the interlayer space. Vermiculites have a similar layer structure and differ from
51 smectites by their higher layer charge deficit [1.2–1.8 and 0.4–1.2 charge equivalent per
52 $\text{O}_{20}(\text{OH})_4$ in vermiculites and smectites, respectively – Guggenheim et al. (2006)]. This charge
53 contrast does not appear to induce significant modification of the hydration behavior or of the
54 distribution of interlayer species (Dazas et al., 2015; Vinci et al., 2020). Both families of swelling
55 phyllosilicates are thus hereafter jointly referred to as “smectite”. The classification of smectite
56 minerals is based on multiple criteria and takes into account the tri- or dioctahedral character
57 of the octahedral sheets, the location of the layer charge (tetrahedral or octahedral), and the
58 density of the layer charge (Guggenheim et al., 2006). For example, saponite is a trioctahedral
59 smectite with tetrahedral layer charge, hectorite is a trioctahedral smectite with octahedral
60 layer charge, and montmorillonite is a dioctahedral smectite with octahedral layer charge. The
61 density and location of the layer charge influences not only smectite cation uptake capacity
62 and the relative affinity of different cations for its surface, but also smectite hydration properties
63 (Sato et al., 1992; Vinci et al., 2020). In turn, hydration and dehydration properties influence
64 smectite swelling and shrinkage properties (e.g. Norrish, 1954). Indeed, smectite hydration
65 involves the uptake of interlayer water, i.e. the intercalation of a variable number of water
66 molecules in the initially anhydrous interlayer (hereafter referred to as the “0W” state). These
67 water molecules are organized to form 1, 2, or 3 “planes” parallel to the layer plane (hereafter
68 denominated “1W”, “2W”, and “3W”, respectively), with the most hydrated interlayer having the
69 highest number of “water planes” and the highest layer-to-layer distance. These interlayer
70 hydration states often coexist within a given crystal, and the structure is then described as
71 “interstratified”, with distinct interlayer spaces hosting different number of water planes. The
72 quantitative understanding of clay hydration thus requires not only the modelling of the total
73 amount of water sorbed as a function of the relative humidity, but also the quantification of the
74 relative abundances of the different hydration states. This ability to model clay hydration is a

75 fundamental stage in the development of THMC (Thermal–Hydraulic–Mechanical–Chemical)
76 codes, which aim to couple chemistry, thermal, hydraulic and mechanical effects to be as
77 realistic as possible, and thus require the link between layer charge and hydration to be
78 quantitatively assessed.

79 To describe the water desorption/adsorption isotherms on clays, numerous studies used the
80 solid solution model based on Ransom and Helgeson (1994) (e.g. Dubacq et al., 2009;
81 Gailhanou et al., 2017; Tajeddine et al., 2015; Vidal and Dubacq, 2009; Vieillard et al., 2011,
82 2019). Although solid solutions, or the consideration of discretized clay end-members with
83 different hydration states, can be employed to describe the water content of clays, the practical
84 implementation of this approach in reactive transport codes remains difficult. These models
85 require indeed the thermodynamic properties of each end-member to be known, i.e. each
86 hydration state, for each layer charge and each interlayer cation, has to be characterized
87 together with possible interaction parameters between end-members (e.g. Margules
88 parameters). Furthermore, most of these models focus on clay formation or stability, and
89 therefore include thermodynamic properties of clay layers (i.e. standard Gibbs energy of
90 formation). As changes in hydration state are relatively rapid processes (e.g. Bray et al., 1998),
91 solid solutions that relate the stability of clay layers are thus incompatible with the use of
92 kinetics driving slow dissolution/precipitation rates of clay minerals (e.g. Marty et al., 2018).
93 Another drawback of the solid solution approach when applied to geochemical modelling is the
94 requirement for the cross-linked thermodynamic equilibrium of both the clay layer and the
95 interlayer cation composition with the contacting solution. As an alternative to these
96 thermodynamic models, Freundlich's model and the BET model (Brunauer, Emmett and Teller)
97 (e.g. Hatch et al., 2012; Revil and Lu, 2013), as well as other equations described in Arthur et
98 al. (2016), are commonly used to reproduce clay desorption/adsorption isotherms. Despite
99 significant efforts (e.g. Lindholm et al., 2019), the lack of mechanistic constraints relating the
100 chemical properties of clay makes the Mechanical–Chemical coupling uncertain, however.
101 Most limitations of the above-described modelling approaches can be circumvented by

102 molecular modelling techniques, which are increasingly used to study the conformation of
103 atoms in the structure (e.g. Dazas et al., 2015; Ferrage et al., 2011), including the dynamics
104 of interlayer cations and water (e.g. Holmboe and Bourg, 2014; Rotenberg et al., 2007).
105 Despite its numerous advantages (sound mechanistic foundations, capacity to probe the
106 kinetics of ion exchange, capacity to predict), the large computational expense required makes
107 molecular modelling incompatible with large scale reactive transport simulations.

108 The present study aims to develop an alternative model focused on clay reactivity (i.e.
109 hydration and cation exchange) which is both numerically robust and easy to implement in
110 geochemical codes, for example to reproduce diagenetic processes (e.g. Tremosa et al.,
111 2020), soil shrink-swell (e.g. Cornelis et al., 2006), soil water availability (e.g. Rawls et al.,
112 1991) or the fate of clays at a radioactive waste disposal site (e.g. Marty et al., 2014). The
113 proposed model is based on the Gapon convention (Gapon, 1933) and uses the exchange
114 reaction formalism (i.e. approach similar to an ideal solid solution) to quantitatively reproduce
115 water desorption isotherms, including total water content and clay hydration heterogeneity (i.e.
116 proportions of 0W, 1W, 2W, and 3W hydrates within a given crystal). It also takes into account
117 the density and location of the layer charge deficit (octahedral or tetrahedral) and the nature
118 of the interlayer cation. As it is based on the exchange convention, this model makes it possible
119 to reproduce quantitatively cation exchange reactions. It was validated against a variety of
120 experimental datasets, including desorption isotherms of two saponites and two hectorites with
121 contrasting layer charges and of Wyoming montmorillonite (SWy-1) with various interlayer
122 compositions (Na and Ca). The present model is satisfactory from a phenomenological point
123 of view as water is presumed to have a specific affinity for each cation and is not considered
124 as an independent parameter, as in many alternative models. Finally, the hydrated exchange
125 models were compared to the classic exchange approach, which conventionally involves
126 anhydrous reactions, and data extracted from experiments involving clay in contact with saline
127 solutions.

128

129 **1. Materials and methods**

130 **1.1. Background**

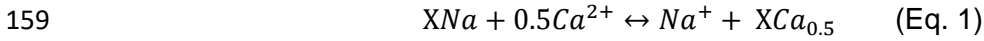
131 A hydrated smectite powder has three different water “reservoirs” (e.g. see figure 1 in
132 Gailhanou et al., 2017). The main one is the interlayer space, where water molecules are
133 hydrating interlayer cations to different degrees (i.e. hydration sphere) according to layer
134 charge, nature of interlayer cation, temperature, and relative humidity (e.g. Dazas et al., 2015).
135 The other two reservoirs are the “external water”, distributed across the external surfaces of
136 clay tactoids (composed of a variable number of stacked layers) (Salles, 2006), and the pore
137 water, located between the clay aggregates (built of connected clay tactoids). Pore water was
138 not accounted for in the present study owing to its negligible role in clay swelling. Moreover,
139 the distinction between interlayer and external water was not made in the present study.
140 Indeed, only interlayer water was required to reproduce water isotherms up to a relative
141 humidity of ~60-70 %, in agreement with previous X-ray diffraction, neutron diffraction, and
142 molecular modelling studies (Ferrage et al., 2005a, 2010, 2011; Vinci et al., 2020). A low
143 contribution of external water in such conditions was also supported by Lindholm et al. (2019).
144 Its contribution is only significant in the relative humidity range where pore water is also
145 present.

146

147 **1.2. Hydrated exchange reactions**

148 The geochemical selectivity constant that relates the amount of a given species in solution with
149 those adsorbed on the solid depends on the water content of the studied material (e.g. Redinha
150 and Kitchener, 1963; Steck and Yeager, 1980). Regarding clay minerals, Tardy and Duplay
151 (1992) described a dependency of the Na/Ca exchange reaction on the number of water
152 molecules. Similarly, Whittaker et al. (2019) have proposed a Na/K exchange model in which
153 the number of water planes was correlated to water activity. To take into account this effect,
154 the Gapon convention (Gapon, 1933) was used here to model the ion exchange reactions

155 involving water molecules in the interlayer space. This convention expresses exchange
 156 reaction per mol of exchange sites rather than per mol of exchanging ion (Gaines and Thomas,
 157 1953). For monovalent Na^+ and bivalent Ca^{2+} cations, the reaction is thus written in the
 158 following way:



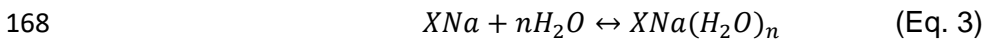
160 where X^- represents the exchanger to which Na^+ or Ca^{2+} cation is bound.

161 The distribution of species is given by the law of mass action:

$$162 \quad K_{\text{Na/Ca}} = \frac{E_{X\text{Ca}_{0.5}}}{E_{X\text{Na}}} \times \frac{[\text{Na}^+]}{[\text{Ca}^{2+}]^{0.5}} \quad (\text{Eq. 2})$$

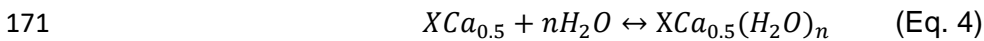
163 where $K_{\text{Na/Ca}}$ is the selectivity constant of the reaction (Eq. 1), E referring to the equivalent
 164 fraction of species on the exchanger and brackets referring to the activity of Na^+ or Ca^{2+} in
 165 solution.

166 In the following, hydration reactions were defined in reference to the dry state. Hydration
 167 reactions involving Na^+ then write:



169 where n is the number of water molecules in the interlayer space per layer charge.

170 For bivalent cations such as Ca^{2+} , the hydration reactions are written as follows:



172 Following the Gapon convention, the general expression of mass action laws for hydration
 173 reactions is:

$$174 \quad K_W = \frac{E_{X\text{Cation}(\text{H}_2\text{O})_n}}{E_{X\text{Cation}}} \times \frac{1}{[\text{H}_2\text{O}]^n} \quad (\text{Eq. 5})$$

175 where K_W is the thermodynamic constant of the hydration reaction (Eq. 3 or 4) and $X\text{Cation}$
 176 refers to $X\text{Na}$ (Eq. 3) or $X\text{Ca}_{0.5}$ (Eq. 4).

177 The definition of Eq. 3-5 illustrates interactions between water, the clay layer and interlayer
178 cation. If necessary, the previous equation (Eq. 5) can be modified according to the Rothmund-
179 Kornfeld description (Bond, 1995):

$$180 \quad K_W = \frac{E_{XCation(H_2O)n}}{E_{XCation}} \times \left(\frac{1}{[H_2O]} \right)^\beta \quad (\text{Eq. 6})$$

181 where β is an empirical parameter. Note that Gapon and Rothmund-Kornfeld approaches are
182 equivalent for $\beta = n$.

183

184 **1.3. Modelling strategy**

185 The calculations were performed with PHREEQC3 (Parkhurst and Appelo, 2013) and the
186 thermodynamic database THERMOCHEM version 9a (Blanc et al., 2015; Giffaut et al., 2014).

187 The simulations of water vapor sorption isotherms required the definition of pore water since
188 the involved chemical reactions do not occur nor can be described in the absence of solvent.

189 The cation concentration in pore water was set at 1 meq L⁻¹ (i.e. solutions containing NaCl,
190 CaCl₂ or NaCl/CaCl₂, with Cl concentration = 1 mmol L⁻¹). The salinity of the pore water was

191 then adjusted by imposing a partial pressure of H₂O(g) to control water activity. In addition, for
192 a solution containing both Na⁺ and Ca²⁺ aqueous species, the increase in the ionic strength of

193 the solution modifies the cationic composition of the exchanger (e.g. Appelo and Postma, 2004;
194 Fletcher and Sposito, 1989). To overcome this effect and reach conditions expected for water

195 adsorption/desorption experiments, an extremely low quantity of pore water can be set in the
196 system (i.e. < 0.1 g H₂O for 1 g of clay). In doing so, the quantity of cations present outside the

197 smectite is much smaller than inside the interlayer spaces and the effect of salinity on the
198 cationic composition of the exchanger can thus be disregarded. The initial Na⁺/Ca²⁺ interlayer

199 population is then independent of relative humidity, as expected during measurements of water
200 vapor sorption isotherms. Furthermore, as the water activity is set in the models [set partial

201 pressure of H₂O(g)] and the effect of salinity on exchangeable cations can be disregarded,
202 simulations of water vapor isotherms do not require the use of activity coefficient corrections

203 dedicated to high salinities, such as the Pitzer equations and their associated databases (e.g.
204 Lach et al., 2018; Lassin et al., 2018).

205

206 **1.4. Data selection**

207 The water contents obtained along the adsorption branch of the isotherms are systematically
208 lower than those measured during desorption (e.g. Bérend et al., 1995; Cases et al., 1992;
209 Ferrage et al., 2010; Lindholm et al., 2019), as the result of various and complex processes
210 (e.g. Woodruff and Revil, 2011) that disfavor water uptake. In the macroscopic approach
211 proposed here, this could be addressed by using an energetic barrier corresponding to the
212 energy required to re-expand the layer-to-layer distance. In addition, clay hydration along the
213 desorption branch of the isotherms appears to be more homogeneous compared to the
214 sorption branch (e.g. Bérend et al., 1995). Consequently, simulations focused on desorption
215 branch of the isotherms for which no energetic barrier is involved.

216 Water desorption data of three different smectite minerals (saponite, hectorite, and
217 montmorillonite) were taken from the literature. They were selected based on (i) the purity of
218 investigated samples, (ii) data quality, and (iii) availability of results from complementary
219 methods (e.g. X-ray diffraction) that allowed quantifying the relative proportion of the different
220 hydration states. For saponite, data from Ferrage et al. (2010) were used. This study provides
221 data for two samples containing interlayer Na and differing in their tetrahedral charge [0.8 and
222 1.4 charge equivalent per $O_{20}(OH)_4$]. These two samples are hereafter referred to as S- $Na_{0.8}$
223 and S- $Na_{1.4}$, respectively. For hectorite, we used data from Vinci et al. (2020). These authors
224 studied the hydration of several sodium hectorites having octahedral charges ranging from 0.8
225 (hereinafter referred to as H- $Na_{0.8}$) to 1.6 (hereinafter referred to as H- $Na_{1.6}$) equivalent per
226 $O_{20}(OH)_4$. Finally, for montmorillonite, the Wyoming montmorillonite (SWy-1) with a charge
227 deficit of 0.74 equivalent per $O_{20}(OH)_4$ (e.g. Cases et al., 1992), mainly located in the
228 octahedral sheet (e.g. Sato et al., 1992), was selected. The SWy-1 was used to study the effect

229 of the interlayer cation nature (Na, Ca, and mixed Na/Ca) on water desorption isotherms. For
 230 this natural sample, changes of hydration state (e.g. from 2W to 1W) are less marked than
 231 those observed with synthetic materials listed above, possibly as the result of an increased
 232 surface charge heterogeneity compared to synthetic saponites and hectorites. Up to 3 water
 233 layers (3W) have been identified at highest relative humidities for hectorite (Vinci et al., 2020)
 234 and montmorillonite (Cases et al., 1992; Holmboe et al., 2012). Dazas et al. (2014) showed
 235 that the 3W layer cannot be described as 3 perfectly discrete planes, but that part of its
 236 interlayer water has some characteristics of the bulk water. Overall, we assumed that the 3W
 237 layer is involved in the crystalline swelling rather the osmotic swelling (e.g. Madsen and Müller-
 238 Vonmoos, 1989; Norrish, 1954) and therefore, we considered it in our modelling exercise.

239

240 **2. Results**

241 **2.1. Effect of smectite tetrahedral layer charge (saponite)**

242 The total amount of water incorporated in S-Na_{0.8} as a function of relative humidity (Figure 1a)
 243 and the corresponding relative proportions of the different hydration states (Figure 1b),
 244 extracted from Ferrage et al. (2010), show that the total interlayer water content is correlated
 245 to the variation in the proportions of 0W, 1W and 2W interlayer hydration states.

246 *Table 1. Reactions and selectivity constants used to simulate the dehydration of saponites S-Na_{0.8} and*
 247 *S-Na_{1.4}. For 1 g of S-Na_{0.8}, a charge deficit of 0.8 eq mol⁻¹ and a molar mass of 776 g mol⁻¹ (Ferrage et*
 248 *al., 2010), the exchanger quantity is 10⁻³ mol. For 1 g of S-Na_{1.4}, a charge deficit of 1.4 eq mol⁻¹ and a*
 249 *molar mass of 789 g mol⁻¹ (Ferrage et al., 2010), the exchanger quantity is 1.8 10⁻³ mol.*

Clay	Reaction	Thermodynamic constant (log K _w)	Description
S-Na _{0.8}	XNa + 5H ₂ O = XNa(H ₂ O) ₅	7	Exchange reaction involving 1 water layer (1W)
	XNa + 12H ₂ O = XNa(H ₂ O) ₁₂	9	Exchange reaction involving 2 water layers (2W)
S-Na _{1.4}	XNa + 2.8H ₂ O = XNa(H ₂ O) _{2.8}	6.3	Exchange reaction involving 1 water layer (1W)

$XNa + 6.7H_2O = XNa(H_2O)_{6.7}$	8	Exchange reaction involving 2 water layers (2W)
-----------------------------------	---	---

250

251 S-Na_{0.8} data were reproduced using the reactions and selectivity constants listed in Table 1. It
 252 was assumed that the species corresponding to 0 water layers did not involve water molecules
 253 (XNa in Table 1), although water molecules bound to the interlayer cation likely persist even
 254 at the lowest relative humidity (e.g. Bérend et al., 1995; Cases et al., 1992; Kloprogge et al.,
 255 1992; Rinnert et al., 2005).

256 The quantity of water in the 1W (Table 1) was estimated to $5 \cdot 10^{-3}$ mol H₂O g⁻¹ of clay, using
 257 the Figure 7 in Ferrage et al. (2010). Interestingly, this value is independent of the cation
 258 exchange capacity (CEC), an observation supported by Dazas et al. (2015). Consequently,
 259 the amount of water to be considered in hydration reaction (Eq. 3) was corrected by the total
 260 exchangeable quantity following:

261
$$n_{1W} = \frac{5 \cdot 10^{-3} \times m_{clay}}{n_{XNa}} \quad (\text{Eq. 7})$$

262 where m_{clay} is the clay mass considered in the numerical simulation and n_{XNa} is the
 263 corresponding exchanger quantity (in moles).

264 For 1 g of clay, a charge deficit of 0.8 equivalent per mole of clay and a molar mass of 776 g
 265 mol⁻¹ (Ferrage et al., 2010), the exchanger quantity is 10^{-3} mol and one obtain $n_{1W} = 5$.

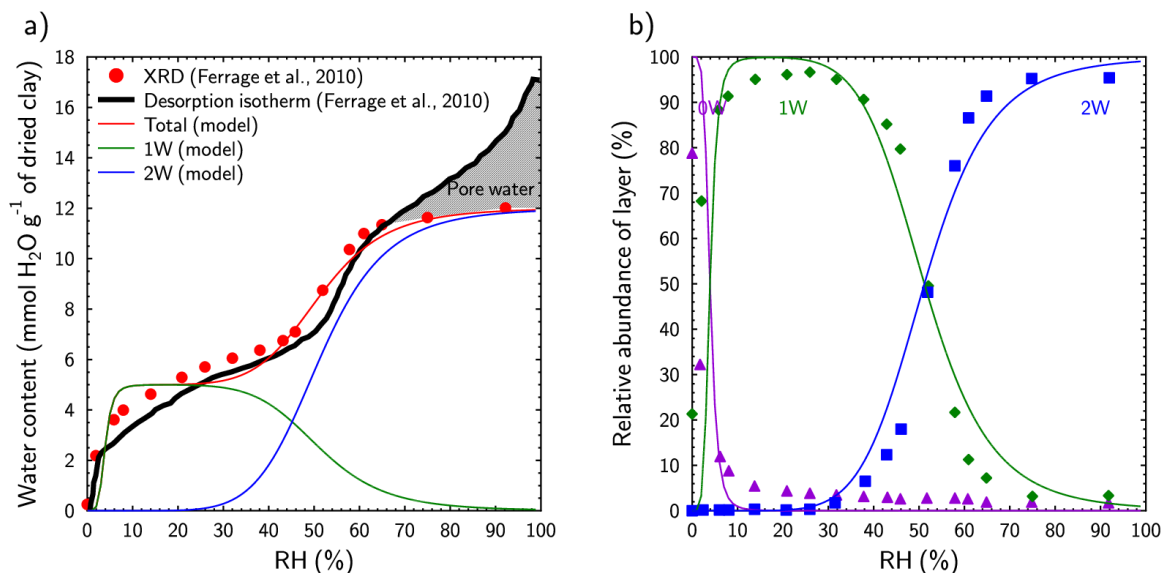
266 Likewise, for 2 water layers (2W in Table 1), we found:

267
$$n_{2W} = \frac{12 \cdot 10^{-3} \times m_{clay}}{n_{XNa}} = 12 \quad (\text{Eq. 8})$$

268 Overall, amounts of water calculated for 1W and 2W reactions agree with several works,
 269 including molecular modelling techniques (e.g. Dazas et al., 2014; Ferrage et al., 2011;
 270 Holmboe and Bourg, 2014). Both the desorption isotherm of Ferrage et al. (2010) and the
 271 relative contribution of the different types of layers were satisfyingly modelled (Figure 1) with
 272 these parameters and refined selectivity constants (Table 1 and electronic annex S-Na0.8.pqi).

273 The misfit at the highest relative humidity (grey area in Figure 1a) in the desorption isotherm
274 was due to the presence of pore water (Ferrage et al., 2010; Salles et al., 2013) which was not
275 considered in this study.

276



277

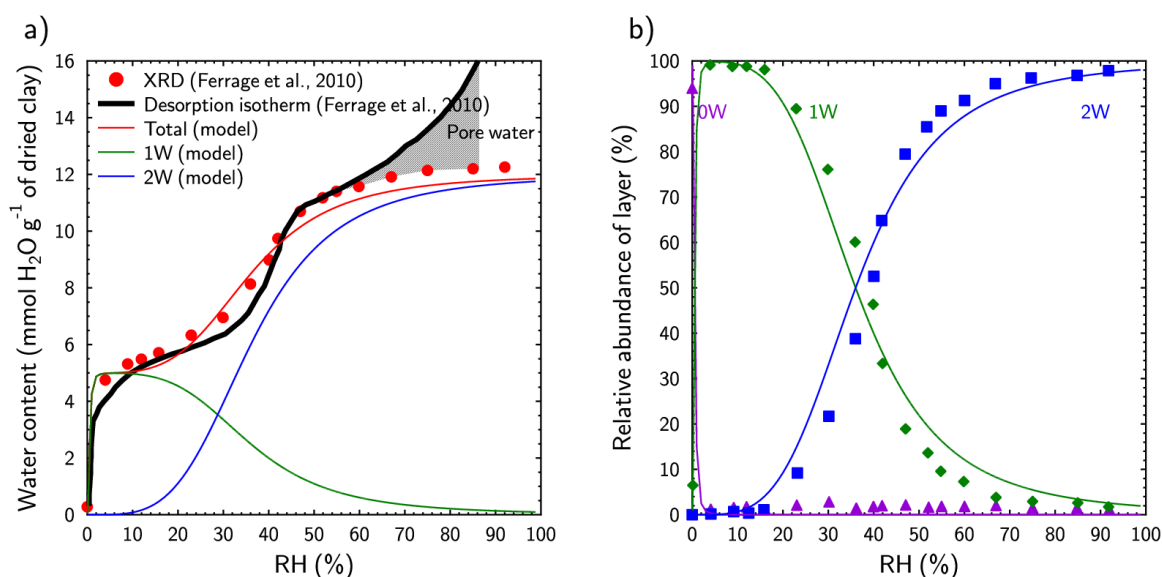
278 *Figure 1. a) comparison of water contents derived from modelling of the XRD profile (red circles) with*
279 *those determined from the water vapor desorption isotherms (black curve). Taken from Ferrage et al.*
280 *(2010) for the saponite S-Na_{0.8}. The green and blue curves indicate the quantity of water modelled for 1*
281 *and 2 layers (1W and 2W, respectively). The red curve represents the total quantity of water modelled*
282 *(Total = 1W + 2W). b) evolution of the relative contribution of the different types of layers (0W, 1W and*
283 *2W) as a function of relative humidity for the saponite S-Na_{0.8}. Symbols: experimental data from Ferrage*
284 *et al. (2010). Curves: numerical results. Purple, green, and blue colors are respectively used for 0W,*
285 *1W, and 2W.*

286

287 Parameters and selectivity coefficients describing the hydration reaction of S-Na_{1.4} were
288 determined as for S-Na_{0.8} and are shown in Table 1. Selectivity constants required further
289 adjustment owing to the change in the number of water molecules involved in the hydration
290 reactions (Eq. 3). As for S-Na_{0.8}, both the desorption isotherms (Figure 2a) and the relative

291 contribution of the different types of layers (0W, 1W and 2W - Figure 2b) as a function of
 292 relative humidity quantitatively reproduced the experimental data of Ferrage et al. (2010). Our
 293 modelling accounted also for the observed broadening of the transition zone between 1W and
 294 2W hydration states, which was due to a decrease of the exponents involved in mass action
 295 equations (2.8 and 6.7 for 1W and 2W reactions, respectively – see Eq. 5 and Table 1).
 296 Together with the data from S-Na_{0.8}, this successful data modelling showed that Gapon
 297 approach can model and predict Na-saponite hydration.

298



299

300 *Figure 2. a) comparison of water contents derived from modelling of the XRD profile (red circles) with*
 301 *those determined from the water vapor desorption isotherms (black curve). Taken from Ferrage et al.*
 302 *(2010) for the saponite S-Na_{1.4}. The green and blue curves indicate the quantity of water modelled for 1*
 303 *and 2 layers (1W and 2W, respectively). The red curve represents the total quantity of water modelled*
 304 *(Total = 1W + 2W) b) evolution of the relative contribution of the different types of layers (0W, 1W and*
 305 *2W) as a function of relative humidity for the saponite S-Na_{1.4}. Symbols: experimental data from Ferrage*
 306 *et al. (2010). Curves: numerical results. Same color coding as in Figure 1.*

307

308 **2.2. Effect of smectite octahedral layer charge (hectorite)**

309 In sodium hectorite, and in contrast to saponite, the relative contributions of 0W, 1W, 2W and
 310 3W as a function of relative humidity are independent of amount of layer charge (Vinci et al.,
 311 2020). As a consequence, hydration reactions must make use of equal exponents for water in
 312 the mass action equations independent of layer charge, and the Rothmund-Kornfeld
 313 description (Bond, 1995) is probably the most straightforward for this purpose. The parameters
 314 were constant whatever the layer charge (Table 2) and allowed us to reproduce the
 315 experimental desorption isotherms and the contributions of 0W, 1W, 2W, and 3W for both H-
 316 Na_{0.8} and H-Na_{1.6} (Figure 3). An example of PHREEQC input file is given in Electronic Annex
 317 (see H-Na0.8.pqi). Note that the 3W contribution was significant only at high relative humidity,
 318 where the contribution of pore water was also strong. Fitted parameters for hydration reaction
 319 involving 3W layers are thus fraught with significant uncertainty.

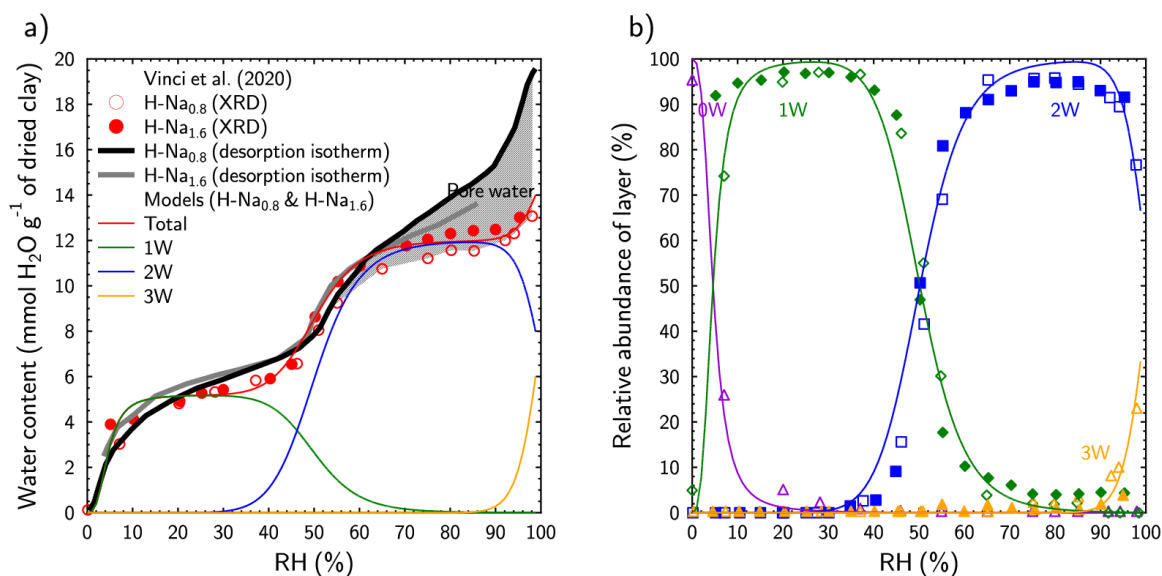
320

321 *Table 2. Reactions and selectivity constants used to simulate the dehydration of hectorites H-Na_{0.8} and*
 322 *H-Na_{1.6}. For 1 g of H-Na_{0.8}, a charge deficit of 0.8 eq mol⁻¹ and a molar mass of 763 g mol⁻¹, the*
 323 *exchanger quantity is 10⁻³ mol. For 1 g of H-Na_{1.6}, a charge deficit of 1.6 eq mol⁻¹ and a molar mass of*
 324 *768 g mol⁻¹, the exchanger quantity is 2 10⁻³ mol.*

Clay	Reaction	Thermodynamic constant (log K _w)	Rothmund-Kornfeld coefficient (β)	Description
H-Na _{0.8}	XNa + 5.2H ₂ O = XNa(H ₂ O) _{5.2}	4	3	Exchange reaction involving 1 water layer (1W)
	XNa + 12H ₂ O = XNa(H ₂ O) ₁₂	7	13.2	Exchange reaction involving 2 water layers (2W)
	XNa + 18H ₂ O = XNa(H ₂ O) ₁₈	6.7	50	Exchange reaction involving 3 water layers (3W)
H-Na _{1.6}	XNa + 2.6H ₂ O = XNa(H ₂ O) _{2.6}	4	3	Exchange reaction involving 1 water layer (1W)
	XNa + 6H ₂ O = XNa(H ₂ O) ₆	7	13.2	Exchange reaction involving 2 water layers (2W)
	XNa + 9H ₂ O = XNa(H ₂ O) ₉	6.7	50	Exchange reaction involving 3 water layers (3W)

325

326



327

328 *Figure 3. a) comparison of water contents derived from modelling of the XRD profile (red circles) with*
 329 *those determined from the water vapor desorption isotherms (black and grey curves). Taken from Vinci*
 330 *et al. (2020) for hectorites H-Na_{0.8} and H-Na_{1.6}. The green, blue and orange curves indicate the quantity*
 331 *of water modelled for 1, 2 and 3 layers (1W, 2W and 3W, respectively) for both H-Na_{0.8} and H-Na_{1.6}. The*
 332 *red curve represents the total quantity of water modelled (Total = 1W + 2W + 3W) for both H-Na_{0.8} and*
 333 *H-Na_{1.6}. b) evolution of the relative contribution of the different types of layers (0W, 1W, 2W and 3W) as*
 334 *a function of relative humidity. Open and fill symbols: experimental data from Vinci et al. (2020) for H-*
 335 *Na_{0.8} and H-Na_{1.6}, respectively. Curves: numerical results. Purple, green, blue and yellow colors are*
 336 *respectively used for 0W, 1W, 2W and 3W.*

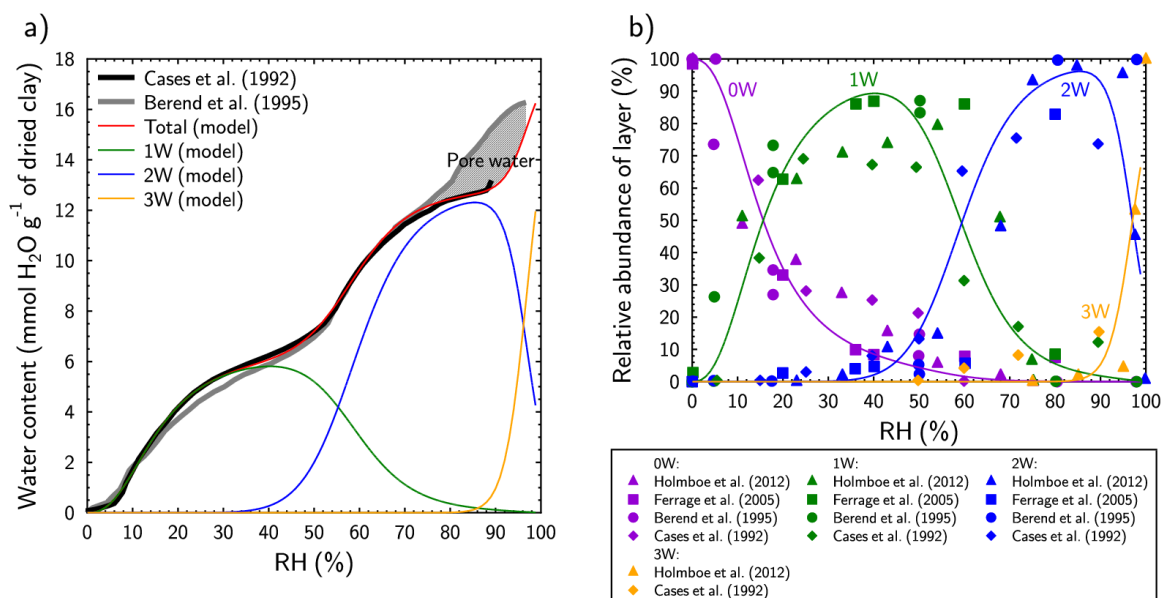
337

338 **2.3. Effect of the type of interlayer cation (SWy-1 smectite)**

339 Experimental desorption isotherms of the Na-exchanged SWy-1, hereafter referred to as Na-
 340 SWy-1 (Figure 4a – Cases et al. (1992), Bérend et al. (1995)), were successfully modelled
 341 using the Rothmund-Kornfeld parameters listed in Table 3. These values allowed also
 342 reproducing the experimentally derived relative contributions of 0W, 1W, 2W, and 3W layers
 343 (Figure 4b). The water contents in 1W and 2W layers were estimated from the desorption
 344 isotherms. 3W layers were also considered in the modelling of the high relative humidity
 345 (Figure 4b), consistent with the reports of Holmboe et al. (2012) and Cases et al. (1992). As

346 for hectorite, parameters refined for exchange reactions involving 3W layers were poorly
 347 constrained owing to the overlap with the pore water contribution (Figure 4a).

348

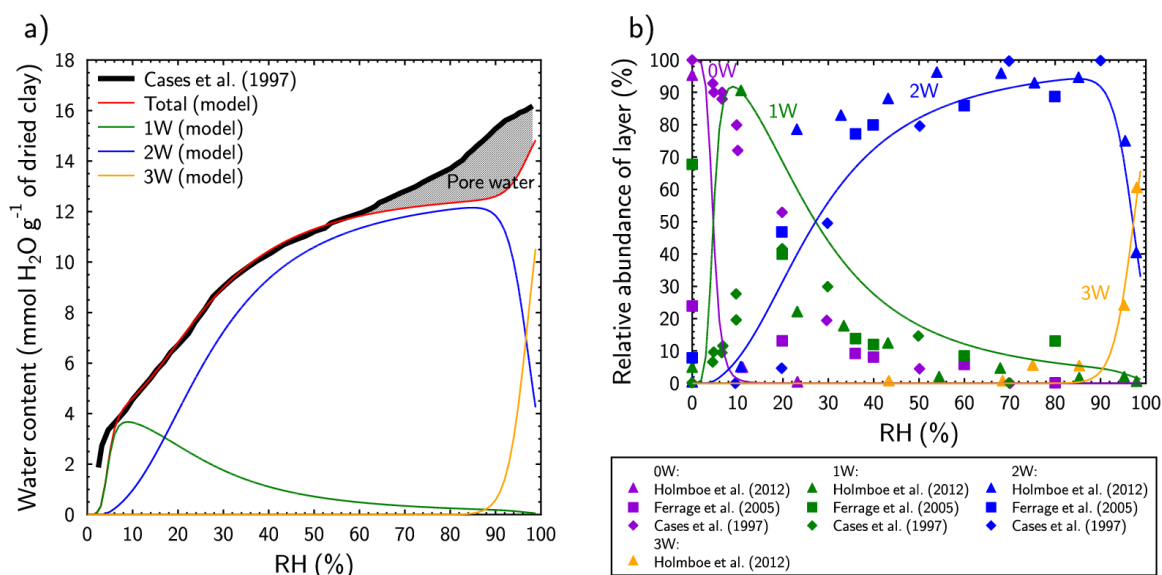


349

350 *Figure 4. a) desorption isotherm obtained for the smectite Na-SWy-1. b) evolution of the relative*
 351 *contribution of the different types of layers (0W, 1W, 2W and 3W) as a function of relative humidity for*
 352 *the smectite Na-SWy-1. Same color coding as in Figure 3.*

353

354 The same modelling procedure was applied to the experimental water desorption isotherm
 355 obtained for Ca-exchanged SWy-1 (Cases et al., 1997), hereafter referred to as Ca-SWy-1. As
 356 for Na-SWy-1, and although the plateaus in the desorption isotherms were less marked, a
 357 satisfying data modelling (with parameters listed in Table 3) could be obtained, both for the
 358 water desorption isotherm (Figure 5a) and for the evolution of the relative number of 0W, 1W,
 359 2W, and 3W layers (Figure 5b). Overall, refined parameters (selectivity constants, Rothmund-
 360 Kornfeld coefficients, water contents for 1W, 2W, and 3W) differed significantly from that
 361 established for Na-SWy-1 (Table 3) due to the hydration behavior of Ca-SWy-1. In contrast to
 362 its Na-exchanged counterpart, 2W hydrates prevailed over a large range of relative humidity
 363 conditions in Ca-SWy-1.



365

366 Figure 5. a) desorption isotherm obtained for the smectite Ca-SWy-1. b) evolution of the relative
 367 contribution of the different types of layers (0W, 1W, 2W and 3W) as a function of relative humidity for
 368 the smectite Ca-SWy-1. Same color coding as in Figure 3.

369

370 Table 3. Reactions and selectivity constants used to simulate the dehydration of smectites Na-SWy-1
 371 and Ca-SWy-1. For 1 g of clay, a charge deficit of 0.74 eq mol^{-1} and a molar mass of 742 g mol^{-1} (Cases
 372 et al., 1992), the exchanger quantity is 10^{-3} mol .

Clay	Reaction	Thermodynamic constant (log Kw)	Rothmund-Kornfeld coefficient (β)	Description
Na-SWy-1	$X\text{Na} + 6.5\text{H}_2\text{O} = X\text{Na}(\text{H}_2\text{O})_{6.5}$	2	2.5	Exchange reaction involving 1 water layer (1W)
	$X\text{Na} + 12.8\text{H}_2\text{O} = X\text{Na}(\text{H}_2\text{O})_{12.8}$	4.1	12	Exchange reaction involving 2 water layers (2W)
	$X\text{Na} + 18\text{H}_2\text{O} = X\text{Na}(\text{H}_2\text{O})_{18}$	4.4	50	Exchange reaction involving 3 water layers (3W)
Ca-SWy-1	$X\text{Ca}_{0.5} + 4\text{H}_2\text{O} = X\text{Ca}_{0.5}(\text{H}_2\text{O})_4$	7.3	5.5	Exchange reaction involving 1 water layer (1W)
	$X\text{Ca}_{0.5} + 12.9\text{H}_2\text{O} = X\text{Ca}_{0.5}(\text{H}_2\text{O})_{12.9}$	8.7	8	Exchange reaction involving 2 water layers (2W)
	$X\text{Ca}_{0.5} + 16\text{H}_2\text{O} = X\text{Ca}_{0.5}(\text{H}_2\text{O})_{16}$	9	50	Exchange reaction involving 3 water layers (3W)

373

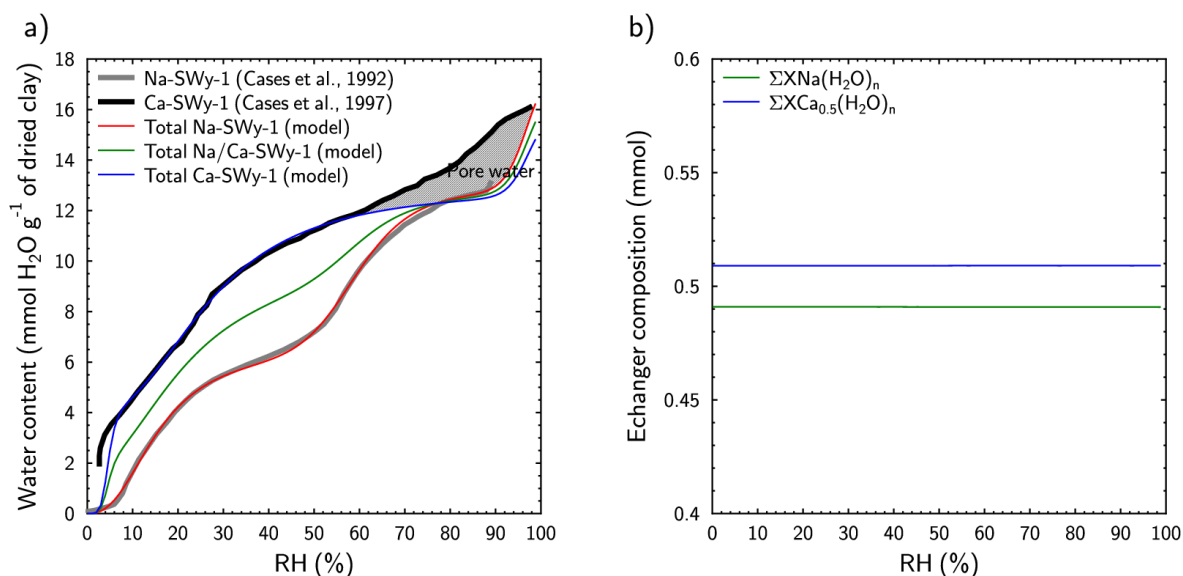
374 **3. Discussion**

375 A dependency on charge location was implemented here in the formalism used here to
376 describe and model hydration reactions. The Gapon formalism was able to predict saponite
377 hydration (S-Na_{0.8} and S-Na_{1.4}), for which the clay layer and interlayer Na⁺, and associated
378 H₂O molecules, are strongly bound owing to the strong undersaturation of layer surface oxygen
379 atoms (i.e. tetrahedral charge, Michot et al., 2005; Prost et al., 1998; Skipper et al., 1990).
380 Further investigations are required however to assess the validity of this model for other cations
381 (e.g. calcium saponite). The Rothmund-Kornfeld description was used for the modelling of
382 hectorite and montmorillonite hydration (H-Na_{0.8}, H-Na_{1.6}, Na-SWy-1 and Ca-SWy-1), for which
383 water molecules interact weakly with the clay layer (i.e. octahedral charge, Doner and
384 Mortland, 1971; Prost et al., 1998; Vinci et al., 2020). The later empirical description may also
385 be used to describe saponite hydration, however, as both Gapon and Rothmund-Kornfeld
386 approaches are equivalent when $\beta = n$ (Eq. 5-6). Regarding ion exchange reactions, the
387 Rothmund-Kornfeld description has been found to be applicable in numerous cases (e.g. Bond
388 and Verburg, 1997; Escudey et al., 2001; Reynolds and Tardiff, 2015). As reported by Bond
389 (1995), it appears more accurate because it avoids extrapolation of the data required for the
390 thermodynamic approach.

391 The capacity of our model to predict the complex hydration behavior of clays exposed to
392 contrasting environmental conditions was evaluated for a smectite interacting with a mixed
393 cation pore water composition using parameters previously established for Na-SWy-1 and Ca-
394 SWy-1 (Table 3). The desorption isotherm calculated for the clay SWy-1 containing ~50% of
395 Na⁺ and ~25% of Ca²⁺ is shown in Figure 6a (green curve). The PHREEQC input file is given
396 in Electronic Annex (see SWy-1_NaCa.pqi). This isotherm was calculated as a simple
397 weighted sum of water layer contributions from Na and Ca end-members. Such an assumption
398 relies on the presence of homoionic interlayers and is supported by numerous works showing
399 a segregation of cations in different interlayers (e.g. Ferrage et al., 2005c; Méring and Glaeser,
400 1954; Möller et al., 2010). Nonetheless, cation de-mixing is a complex phenomenon that

401 depends on several parameters such as the substitution level (Fink et al., 1971) or the layer
 402 charge (Laird, 2006). The desorption isotherm of the smectite Na/Ca-SWy-1 was then found
 403 in between that of the smectite Na-SWy-1 (red curve) and that of Ca-SWy-1 (blue curve). A
 404 similar behavior has been observed by Keren and Shainberg (1979) on the adsorption isotherm
 405 of a mixed Na/Ca Wyoming. Consistent with the adopted simulation approach (see section
 406 1.3), and as expected during an isotherm measurement, the proportion of Na and Ca in the
 407 interlayer space was independent of relative humidity (Figure 6b).

408



409

410 *Figure 6. a) desorption isotherms obtained for the smectites Na-SWy-1, Ca-SWy-1 and Na/Ca-SWy-1.*
 411 *b) exchanger composition as a function of relative humidity for the smectite Na/Ca-SWy-1 (calculation*
 412 *performed without pore water, see text).*

413

414 The proposed model allowed also predicting the effect of solution salinity on the interlayer
 415 composition of the SWy-1 (Figure 7). In accordance with the cation exchange data of Gaucher
 416 et al. (2009), the selectivity constant of the anhydrous Na/Ca exchange reaction (Eq. 1) was
 417 equal to 0.35 (log unit). At lowest salinities, the presence of most hydrated species (i.e. 3W
 418 hydration reactions reported in Table 3) were expected from previous considerations, however,

419 and thermodynamic exchange constant must be corrected when Eq. 1 is coupled with Eq. 3-
420 4:

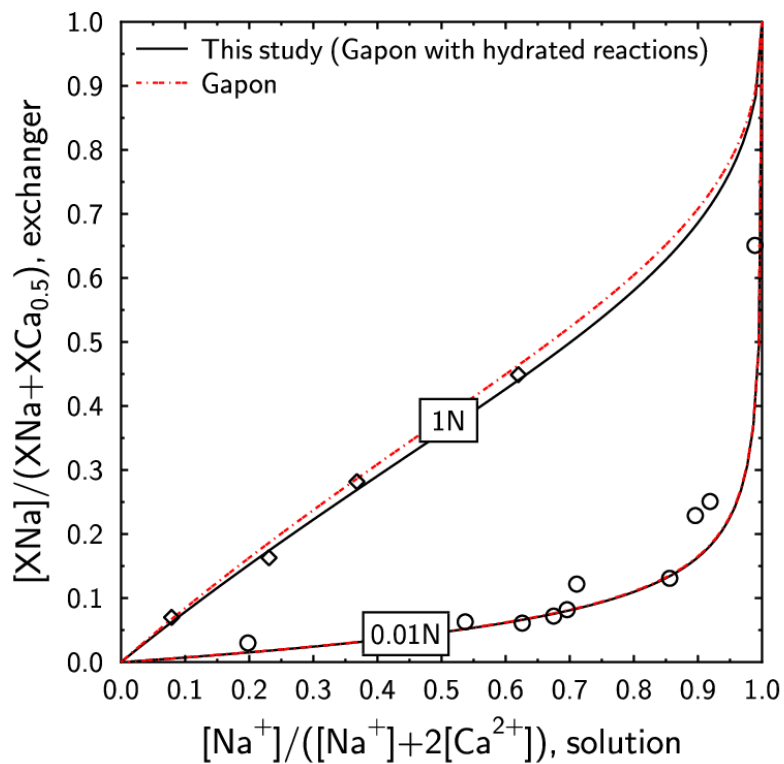
$$421 \quad \text{Log } K_{Na/Ca}^{hydrated} = \text{Log } K_{3W}^{Na-SWy-1} - \text{Log } K_{3W}^{Ca-SWy-1} + \text{Log } K_{Na/Ca}^{anhydrous} \quad (\text{Eq. 9})$$

422 where $K_{Na/Ca}^{hydrated}$ is the selectivity constant for hydrated Na/Ca exchange reaction, $K_{3W}^{Na-SWy-1}$
423 the thermodynamic constant of the 3W hydration reaction involving the Na-SWy-1 (Table 3),
424 $K_{3W}^{Ca-SWy-1}$ the thermodynamic constant of the 3W hydration reaction involving the Ca-SWy-1
425 (Table 3) and $K_{Na/Ca}^{anhydrous}$ the selectivity constant of the anhydrous Na/Ca exchange reaction
426 ($10^{0.35}$).

427 The Na/Ca exchange isotherm has been calculated for total Na and Ca concentrations of 0.01
428 and 1 mol L⁻¹ (Cl⁻ as charge-compensating anion). As showed in numerous studies (e.g. Appelo
429 and Postma, 2004; Fletcher and Sposito, 1989), calculations depend on the exponent used in
430 the mass action equation (Eq. 2) and thus the content of adsorbed Ca²⁺ increases with the
431 decrease of the ionic strength. The exchange isotherms obtained with the Gapon convention
432 involving anhydrous and hydrated reactions (Eq. 1 vs. Eq. 1, 3-4) overlapped for 0.01 mol L⁻¹
433 concentrations (Figure 7), whereas a minor effect of salinity on the apparent selectivity
434 coefficient was observed for 1 mol L⁻¹ concentrations, which is the validity limit of the B-dot
435 activity model (Trémosa et al., 2014). Such discrepancy was due to the non-parallel evolution
436 in water layer contributions from Na and Ca end-members with increasing ionic strength; as
437 cation exchange and hydration reactions are coupled, clay hydration state affects in turn the
438 exchange reaction through a feedback effect. This is supported by several works (e.g. Laird
439 and Shang, 1997; Van Loon and Glaus, 2008; Whittaker et al., 2019). Note that a concentration
440 of 1 mol L⁻¹ is equivalent to 95.6 and 94.2% of relative humidity in NaCl and CaCl₂ type
441 solutions, respectively. Salinity range investigated thus corresponded to the domain where a
442 high contribution of 3W was expected (Figure 4 and Figure 5). Despite 3W reactions being
443 weakly constrained (see section 2.3), the exchange isotherms modelled at 0.01 and 1 mol L⁻¹
444 reproduced the data, even for low salinity and high Na contents (Figure 7). Moreover, at high

445 ionic strengths, formation of CaCl^+ ionic pairs and their incorporation in the interlayer space
446 should ideally be taken into account (Ferrage et al., 2005b; Tertre et al., 2011; Tournassat et
447 al., 2011). As initial first approximation, the exchange of this complex was disregarded in our
448 simulations.

449



450

451 *Figure 7. Comparison of Na/Ca exchange isotherms obtained using anhydrous and hydrated reactions*
452 *for total Na and Ca concentrations (i.e. $[\text{Na}]+[\text{Ca}]$) from 0.01 to 1 mol L⁻¹. The open circles and diamonds*
453 *refer to the experimental data obtained by Tang and Sparks (1993) and Amrhein and Suarez (1991) for*
454 *the smectite SWy-1 at 0.01 and 1 mol L⁻¹, respectively.*

455

456 **4. Implications**

457 The proposed approach does not require the thermodynamic properties of formation of the
458 solids (i.e. clay layers) to be quantified, thus offering greater flexibility, and making it easier to
459 include these models in complex, dynamic systems like soils and sediments. An issue
460 hampering the inclusion of phyllosilicate hydration models in geochemical models resides in
461 the fact that clays, and more especially smectite minerals, have exchangeable interlayer ions.
462 These exchange reactions influence in turn clay hydration behavior (Bérend et al., 1995; Cases
463 et al., 1997). Cation exchanges can be dealt with using non-ideal solid solutions including
464 specific parameters such as Margules parameters (Pabalan, 1994), but most studies dealing
465 with cationic exchange use simpler Gaines and Thomas (1953), Gapon (1933) or Vanselow
466 (1932) formalisms, that involve fewer parameters. These models proved to be extremely robust
467 and efficient for predicting cation migration in clay rocks (Tournassat et al., 2015). The
468 developed approach to predict clay hydration is comparable to that established to quantify and
469 predict cation exchanges in interlayer spaces and sorption on clay edges, which is known as
470 'surface complexation'. In addition, the developed model could be complemented with a
471 surface complexation model to account for external water, based, for instance, on the work of
472 Prost et al. (1998) and/or Lindholm et al. (2019). Such approach would allow refining water
473 balance calculation in reactive transport modelling and coupling more accurately the feedback
474 of chemistry on flow. The importance of such a coupling has been discussed by Seigneur et
475 al. (2018).

476 The coupling between hydration and exchange reactions could be also considered to study
477 the evolution of apparent selectivity constants with the increase of the ionic strength (e.g. Liu
478 et al., 2004). Finally, the hysteresis of water sorption onto clays (e.g. Cases et al., 1992) could
479 be addressed using an energy barrier, the transition from a weakly hydrated species to a highly
480 hydrated species (e.g. from 1W to 2W) then requiring more energy than the opposite reaction.
481 The consideration of an energy barrier could be similar to what is done for a mineral
482 precipitation beyond an over saturation window. In water-saturated conditions and in presence

483 of different cations (e.g. Na⁺ and K⁺, the last one leading to weakly hydrated clay), this energy
484 barrier could induce also an exchange hysteresis (Laird and Shang, 1997), that remains to be
485 thoroughly investigated.

486

487 **Conclusion**

488 The proposed modelling approach allows reproducing satisfactorily experimentally derived
489 water vapor desorption isotherms as well as the different clay hydration states for contrasting
490 charge deficits located in both tetrahedral and octahedral positions. Mass action equations
491 derived from the Gapon convention are well-suited to describe clay hydration involving strong
492 interactions between water molecules and the clay layer (i.e. tetrahedral charge). In contrast,
493 the Rothmund-Kornfeld description may be used whatever the location of the layer charge
494 deficit (tetrahedral or octahedral).

495 The proposed approach, based on an exchange model, is very easy to implement in
496 geochemical codes and is satisfactory from a phenomenological point of view. Consistent with
497 XRD characterizations of water vapor sorption isotherms, most of water molecules are found
498 in smectite interlayers, whereas the relative proportions of the different smectite hydration
499 states depend on both interlayer composition and relative humidity. The consideration of
500 hydration reactions for the Wyoming bentonite does not indicate significant change on Na/Ca
501 cation exchange within the concentration range studied (i.e. < 1 mol L⁻¹) but further work is
502 required to extend the model to other cations (K⁺, Mg²⁺, Sr²⁺ etc.). In addition, this approach,
503 by distinguishing explicitly the hydration/cation exchange process from the thermodynamic
504 stability of the clay layer, is compatible with the use of reaction kinetics. In the long term, the
505 method put forward here should allow linking chemistry to water content in soils, in clay rocks
506 and mechanics that is swelling pressures.

507

508 **Acknowledgments**

509 The authors thank C. Tournassat for fruitful discussions, Carl I. Steefel for editorial handling
510 and the anonymous reviewers for their constructive remarks. BRGM contributors acknowledge
511 funding by internal research grants (HyDoLa and THERMODDEM projects). ISTerre is part of
512 Labex OSUG@2020 (ANR10 LABX56). BL thanks the CNRS interdisciplinary research
513 program Needs, through its “MiPor” project, for financial support.

514

515 **References**

- 516 Amrhein, C., Suarez, D., 1991. Sodium-calcium exchange with anion exclusion and
517 weathering corrections. *Soil Science Society of America Journal* 55, 698-706.
- 518 Appelo, C.A.J., Postma, D., 2004. *Geochemistry, groundwater and pollution*. CRC press.
- 519 Arthur, E., Tuller, M., Moldrup, P., Jonge, L.W.d., 2016. Evaluation of theoretical and
520 empirical water vapor sorption isotherm models for soils. *Water Resources Research*
521 52, 190-205.
- 522 Bérend, I., Cases, J.M., Francois, M., Uriot, J.P., Michot, L., Masion, A., Thomas, F., 1995.
523 Mechanism of adsorption and desorption of water vapor by homoionic
524 montmorillonites; 2, The Li^+ , Na^+ , K^+ , Rb^+ and Cs^+ - exchanged forms. *Clays and Clay*
525 *Minerals* 43, 324-336.
- 526 Blanc, P., Vieillard, P., Gailhanou, H., Gaboreau, S., Marty, N., Claret, F., Madé, B., Giffaut,
527 E., 2015. ThermoChimie database developments in the framework of cement/clay
528 interactions. *Applied Geochemistry* 55, 95-107.
- 529 Bond, W.J., 1995. On the Rothmund-Kornfeld Description of Cation Exchange. *Soil Science*
530 *Society of America Journal* 59, 436-443.
- 531 Bond, W.J., Verburg, K., 1997. Comparison of Methods for Predicting Ternary Exchange
532 from Binary Isotherms. *Soil Science Society of America Journal* 61, 444-454.

533 Bray, H.J., Redfern, S.A.T., Clark, S.M., 1998. The kinetics of dehydration in Ca-
534 montmorillonite; an in situ X-ray diffraction study. *Mineralogical Magazine* 62, 647-656.

535 Cases, J., Bérend, I., François, M., Uriot, J., Michot, L., Thomas, F., 1997. Mechanism of
536 adsorption and desorption of water vapor by homoionic montmorillonite; 3, The Mg²⁺,
537 Ca²⁺, and Ba³⁺ exchanged forms. *Clays and Clay Minerals* 45, 8-22.

538 Cases, J.M., Berend, I., Besson, G., Francois, M., Uriot, J.P., Thomas, F., Poirier, J.E., 1992.
539 Mechanism of adsorption and desorption of water vapor by homoionic montmorillonite.
540 1. The sodium-exchanged form. *Langmuir* 8, 2730-2739.

541 Cornelis, W.M., Corluy, J., Medina, H., Díaz, J., Hartmann, R., Van Meirvenne, M., Ruiz,
542 M.E., 2006. Measuring and modelling the soil shrinkage characteristic curve.
543 *Geoderma* 137, 179-191.

544 Dazas, B., Ferrage, E., Delville, A., Lanson, B., 2014. Interlayer structure model of tri-
545 hydrated low-charge smectite by X-ray diffraction and Monte Carlo modeling in the
546 Grand Canonical ensemble. *American Mineralogist* 99, 1724-1735.

547 Dazas, B., Lanson, B., Delville, A., Robert, J.-L., Komarneni, S., Michot, L.J., Ferrage, E.,
548 2015. Influence of Tetrahedral Layer Charge on the Organization of Interlayer Water
549 and Ions in Synthetic Na-Saturated Smectites. *The Journal of Physical Chemistry C*
550 119, 4158-4172.

551 Doner, H.E., Mortland, M.M., 1971. Charge Location as a Factor in the Dehydration of 2:1
552 Clay Minerals. *Soil Science Society of America Journal* 35, 360-362.

553 Dubacq, B., Vidal, O., De Andrade, V., 2009. Dehydration of dioctahedral aluminous
554 phyllosilicates: thermodynamic modelling and implications for thermobarometric
555 estimates. *Contributions to Mineralogy and Petrology* 159, 159.

556 Escudey, M., Díaz, P., Förster, J.E., Pizarro, C., Galindo, G., 2001. Gaines–thomas and
557 rothmund–kornfeld descriptions of potassium–calcium exchange on variable surface
558 charge soils. *Communications in Soil Science and Plant Analysis* 32, 3087-3097.

559 Ferrage, E., Lanson, B., Michot, L.J., Robert, J.-L., 2010. Hydration Properties and Interlayer
560 Organization of Water and Ions in Synthetic Na-Smectite with Tetrahedral Layer

561 Charge. Part 1. Results from X-ray Diffraction Profile Modeling. The Journal of Physical
562 Chemistry C 114, 4515-4526.

563 Ferrage, E., Lanson, B., Sakharov, B.A., Drits, V.A., 2005a. Investigation of smectite
564 hydration properties by modeling experimental X-ray diffraction patterns. Part I.
565 Montmorillonite hydration properties. American Mineralogist 90, 1358-1374.

566 Ferrage, E., Sakharov, B.A., Michot, L.J., Delville, A., Bauer, A., Lanson, B., Grangeon, S.,
567 Frapper, G., Jiménez-Ruiz, M., Cuello, G.J., 2011. Hydration Properties and Interlayer
568 Organization of Water and Ions in Synthetic Na-Smectite with Tetrahedral Layer
569 Charge. Part 2. Toward a Precise Coupling between Molecular Simulations and
570 Diffraction Data. Journal of Physical Chemistry C 115, pp.1867-1881.

571 Ferrage, E., Tournassat, C., Rinnert, E., Charlet, L., Lanson, B., 2005b. Experimental
572 Evidence for Ca-Chloride Ion Pairs in the Interlayer of Montmorillonite. an XRD Profile
573 Modeling Approach. Clays and Clay Minerals 53, 348-360.

574 Ferrage, E., Tournassat, C., Rinnert, E., Lanson, B., 2005c. Influence of pH on the interlayer
575 cationic composition and hydration state of Ca-montmorillonite: Analytical chemistry,
576 chemical modelling and XRD profile modelling study. Geochimica et Cosmochimica
577 Acta 69, 2797-2812.

578 Fink, D.H., Nakayama, F.S., McNeal, B.L., 1971. Demixing of Exchangeable Cations in Free-
579 Swelling Bentonite Clay. Soil Science Society of America Journal 35, 552-555.

580 Fletcher, P., Sposito, G., 1989. Chemical modeling of clay/electrolyte interactions of
581 montmorillonite. Clay Minerals 24, 375-391.

582 Gailhanou, H., Vieillard, P., Blanc, P., Lassin, A., Denoyel, R., Bloch, E., De Weireld, G.,
583 Gaboreau, S., Fialips, C.I., Madé, B., Giffaut, E., 2017. Methodology for determining
584 the thermodynamic properties of smectite hydration. Applied Geochemistry 82, 146-
585 163.

586 Gaines, G.L., Thomas, H.C., 1953. Adsorption studies on clay minerals. II. A formulation of
587 the thermodynamics of exchange adsorption. J. Chem. Phys. 21(4), 714-718.

588 Gapon, Y.N., 1933. On the theory of exchange adsorption in soils. *J. Gen. Chern. U.S.S.R.*
589 (Engl. Trans.) 3, 144-160.

590 Gaucher, E.C., Tournassat, C., Pearson, F.J., Blanc, P., Cruzet, C., Lerouge, C., Altmann,
591 S., 2009. A robust model for pore-water chemistry of clayrock. *Geochimica et*
592 *Cosmochimica Acta* 73, 6470-6487.

593 Giffaut, E., Grivé, M., Blanc, P., Vieillard, P., Colàs, E., Gailhanou, H., Gaboreau, S., Marty,
594 N., Madé, B., Duro, L., 2014. Andra thermodynamic database for performance
595 assessment: ThermoChimie. *Applied Geochemistry* 49, 225-236.

596 Griffin, J.J., Windom, H., Goldberg, E.D., 1968. The distribution of clay minerals in the World
597 Ocean. *Deep Sea Research and Oceanographic Abstracts* 15, 433-459.

598 Guggenheim, S., Adams, J.M., Bain, D.C., Bergaya, F., Brigatti, M.F., Drits, V.A., Formoso,
599 M.L.L., Galan, E., Kogure, T., Stanjek, H., 2006. Summary of recommendations of
600 nomenclature committees relevant to clay mineralogy: Report of the Association
601 Internationale pour l'Etude des Argiles (AIPEA) Nomenclature. *Clays and Clay Minerals*
602 54, 761-772.

603 Hatch, C.D., Wiese, J.S., Crane, C.C., Harris, K.J., Kloss, H.G., Baltrusaitis, J., 2012. Water
604 Adsorption on Clay Minerals As a Function of Relative Humidity: Application of BET
605 and Freundlich Adsorption Models. *Langmuir* 28.

606 Holmboe, M., Bourg, I.C., 2014. Molecular Dynamics Simulations of Water and Sodium
607 Diffusion in Smectite Interlayer Nanopores as a Function of Pore Size and
608 Temperature. *The Journal of Physical Chemistry C* 118, 1001-1013.

609 Holmboe, M., Wold, S., Jonsson, M., 2012. Porosity investigation of compacted bentonite
610 using XRD profile modeling. *Journal of Contaminant Hydrology* 128, 19-32.

611 Jackson, M.L., 1957. Frequency Distribution of Clay Minerals in Major Great Soil Groups as
612 Related to the Factors of Soil Formation. *Clays and Clay Minerals* 6, 133-143.

613 Keren, R., Shainberg, I., 1979. Water Vapor Isotherms and Heat of Immersion of Na/Ca-
614 Montmorillonite Systems—II: Mixed Systems. *Clays and Clay Minerals* 27, 145-151.

615 Klopogge, J.T., Jansen, J.B.H., Schuiling, R.D., Geus, J.W., 1992. The interlayer collapse
616 during dehydration of synthetic Na0.7-beidellite: a ^{23}Na solid-state magic-angle
617 spinning NMR study. *Clays and Clay Minerals* 40, 561-566.

618 Lach, A., André, L., Guignot, S., Christov, C., Henocq, P., Lassin, A., 2018. A Pitzer
619 Parametrization To Predict Solution Properties and Salt Solubility in the H–Na–K–Ca–
620 Mg–NO₃–H₂O System at 298.15 K. *Journal of Chemical and Engineering Data* 63, 787
621 - 800.

622 Laird, D.A., 2006. Influence of layer charge on swelling of smectites. *Applied Clay Science*
623 34, 74-87.

624 Laird, D.A., Shang, C., 1997. Relationship Between Cation Exchange Selectivity and
625 Crystalline Swelling in Expanding 2:1 Phyllosilicates. *Clays and Clay Minerals* 45, 681-
626 689.

627 Lassin, A., André, L., Lach, A., Thadée, A.-L., Cézac, P., Serin, J.-P., 2018. Solution
628 properties and salt-solution equilibria in the H-Li-Na-K-Ca-Mg-Cl-H₂O system at 25 °C:
629 A new thermodynamic model based on Pitzer's equations. *Calphad* 61, 126-139.

630 Lindholm, J., Boily, J.-F., Holmboe, M., 2019. Deconvolution of Smectite Hydration
631 Isotherms. *ACS Earth and Space Chemistry*.

632 Liu, C., Zachara, J.M., Smith, S.C., 2004. A cation exchange model to describe Cs⁺ sorption
633 at high ionic strength in subsurface sediments at Hanford site, USA. *Journal of*
634 *Contaminant Hydrology* 68, 217-238.

635 Madsen, F.T., Müller-Vonmoos, M., 1989. The swelling behaviour of clays. *Applied Clay*
636 *Science* 4, 143-156.

637 Marty, N.C.M., Lach, A., Lerouge, C., Grangeon, S., Claret, F., Fauchet, C., Madé, B., Lundy,
638 M., Lagroix, F., Tournassat, C., Tremosa, J., 2018. Weathering of an argillaceous rock
639 in the presence of atmospheric conditions: A flow-through experiment and modelling
640 study. *Applied Geochemistry* 96, 252-263.

641 Marty, N.C.M., Munier, I., Gaucher, E.C., Tournassat, C., Gaboreau, S., Vong, C.Q., Giffaut,
642 E., Cochepin, B., Claret, F., 2014. Simulation of Cement/Clay Interactions: Feedback

643 on the Increasing Complexity of Modelling Strategies. *Transport in Porous Media* 104,
644 385-405.

645 Méring, J., Glaeser, R., 1954. Sur le rôle de la valence des cations échangeables dans la
646 montmorillonite. *Bulletin de Minéralogie*, 519-530.

647 Michot, L.J., Bihannic, I., Pelletier, M., Rinnert, E., Robert, J.-L., 2005. Hydration and swelling
648 of synthetic Na-saponites: Influence of layer charge. *American Mineralogist* 90, 166-
649 172.

650 Möller, M.W., Hirsemann, D., Haarmann, F., Senker, J., Breu, J., 2010. Facile Scalable
651 Synthesis of Rectorites. *Chemistry of Materials* 22, 186-196.

652 Murray, H.H., Leininger, R.K., 1955. Effect of Weathering on Clay Minerals. *Clays and Clay*
653 *Minerals* 4, 340-347.

654 Norrish, K., 1954. The swelling of montmorillonite. *Discussions of the Faraday society* 18,
655 120-134.

656 Pabalan, R.T., 1994. Thermodynamics of ion exchange between clinoptilolite and aqueous
657 solutions of Na^+K^+ and Na^+Ca^{2+} . *Geochimica et Cosmochimica Acta* 58, 4573-4590.

658 Parkhurst, D.L., Appelo, C., 2013. Description of input and examples for PHREEQC version
659 3—a computer program for speciation, batch-reaction, one-dimensional transport, and
660 inverse geochemical calculations. *US geological survey techniques and methods*, book
661 6, 497.

662 Prost, R., Koutit, T., Benchara, A., Huard, E., 1998. State and location of water adsorbed on
663 clay minerals; consequences of the hydration and swelling-shrinkage phenomena.
664 *Clays and Clay Minerals* 46, 117-131.

665 Ransom, B., Helgeson, H.C., 1994. A chemical and thermodynamic model of aluminous
666 dioctahedral 2:1 layer clay minerals in diagenetic processes; regular solution
667 representation of interlayer dehydration in smectite. *American Journal of Science* 294,
668 449-484.

669 Rawls, W.J., Gish, T.J., Brakensiek, D.L., 1991. Estimating Soil Water Retention from Soil
670 Physical Properties and Characteristics, in: Stewart, B.A. (Ed.), *Advances in Soil*
671 *Science: Volume 16*. Springer New York, New York, NY, pp. 213-234.

672 Redinha, J., Kitchener, J., 1963. Thermodynamics of ion-exchange processes. System H, Na
673 and Ag with polystyrene sulphonate resins. *Transactions of the Faraday Society* 59,
674 515-529.

675 Revil, A., Lu, N., 2013. Unified water isotherms for clayey porous materials. *Water*
676 *Resources Research* 49, 5685-5699.

677 Reynolds, J., Tardiff, B., 2015. A Rothmund–Kornfeld model of Cs⁺–K⁺–Na⁺ exchange on
678 spherical resorcinol-formaldehyde (sRF) resin in Hanford nuclear waste. *Journal of*
679 *Radioanalytical and Nuclear Chemistry*.

680 Rinnert, E., Carteret, C., Humbert, B., Fragneto-Cusani, G., Ramsay, J.D.F., Delville, A.,
681 Robert, J.-L., Bihannic, I., Pelletier, M., Michot, L.J., 2005. Hydration of a Synthetic
682 Clay with Tetrahedral Charges: A Multidisciplinary Experimental and Numerical Study.
683 *The Journal of Physical Chemistry B* 109, 23745-23759.

684 Rotenberg, B., Marry, V., Dufrêche, J.-F., Malikova, N., Giffaut, E., Turq, P., 2007. Modelling
685 water and ion diffusion in clays: A multiscale approach. *Comptes Rendus Chimie* 10,
686 1108-1116.

687 Salles, F., 2006. Hydration of swelling clays: multi-scale sequence of hydration and
688 determination of macroscopic energies from microscopic properties. Université Pierre
689 et Marie Curie - Paris VI.

690 Salles, F., Douillard, J.-M., Bildstein, O., Gaudin, C., Prelot, B., Zajac, J., Van Damme, H.,
691 2013. Driving force for the hydration of the swelling clays: Case of montmorillonites
692 saturated with alkaline-earth cations. *Journal of Colloid and Interface Science* 395,
693 269-276.

694 Sato, T., Watanabe, T., Otsuka, R., 1992. Effects of Layer Charge, Charge Location, and
695 Energy Change on Expansion Properties of Dioctahedral Smectites. *Clays and Clay*
696 *Minerals* 40, 103-113.

697 Seigneur, N., Lagneau, V., Corvisier, J., Dauzères, A., 2018. Recoupling flow and chemistry
698 in variably saturated reactive transport modelling - An algorithm to accurately couple
699 the feedback of chemistry on water consumption, variable porosity and flow. *Advances*
700 *in Water Resources* 122, 355-366.

701 Skipper, N.T., Soper, A.K., McConnell, J.D.C., Refson, K., 1990. The structure of interlayer
702 water in a hydrated 2:1 clay. *Chemical Physics Letters* 166, 141-145.

703 Steck, A., Yeager, H., 1980. Water sorption and cation-exchange selectivity of a
704 perfluorosulfonate ion-exchange polymer. *Analytical Chemistry* 52, 1215-1218.

705 Tajeddine, L., Gailhanou, H., Blanc, P., Lassin, A., Gaboreau, S., Vieillard, P., 2015.
706 Hydration–dehydration behavior and thermodynamics of MX-80 montmorillonite studied
707 using thermal analysis. *Thermochimica Acta* 604, 83-93.

708 Tang, L., Sparks, D.L., 1993. Cation-exchange kinetics on montmorillonite using pressure-
709 jump relaxation. *Soil Science Society of America Journal* 57, 42-46.

710 Tardy, Y., Duplay, J., 1992. A method of estimating the Gibbs free energies of formation of
711 hydrated and dehydrated clay minerals. *Geochimica et Cosmochimica Acta* 56, 3007-
712 3029.

713 Tertre, E., Prêt, D., Ferrage, E., 2011. Influence of the ionic strength and solid/solution ratio
714 on Ca(II)-for-Na⁺ exchange on montmorillonite. Part 1: Chemical measurements,
715 thermodynamic modeling and potential implications for trace elements geochemistry.
716 *Journal of Colloid and Interface Science* 353, 248-256.

717 Tournassat, C., Bizi, M., Braibant, G., Cruzet, C., 2011. Influence of montmorillonite tactoid
718 size on Na–Ca cation exchange reactions. *Journal of Colloid and Interface Science*
719 364, 443-454.

720 Tournassat, C., Steefel, C.I., Bourg, I.C., Bergaya, F., 2015. Natural and engineered clay
721 barriers. Elsevier.

722 Trémosa, J., Castillo, C., Vong, C.Q., Kervévan, C., Lassin, A., Audigane, P., 2014. Long-
723 term assessment of geochemical reactivity of CO₂ storage in highly saline aquifers:

724 Application to Ketzin, In Salah and Snøhvit storage sites. *International Journal of*
725 *Greenhouse Gas Control* 20, 2-26.

726 Tremosa, J., Gailhanou, H., Chiaberge, C., Castilla, R., Gaucher, E.C., Lassin, A., Gout, C.,
727 Fialips, C., Claret, F., 2020. Effects of smectite dehydration and illitisation on
728 overpressures in sedimentary basins: A coupled chemical and thermo-hydro-
729 mechanical modelling approach. *Marine and Petroleum Geology* 111, 166-178.

730 Van Loon, L.R., Glaus, M.A., 2008. Mechanical Compaction of Smectite Clays Increases Ion
731 Exchange Selectivity for Cesium. *Environmental Science & Technology* 42, 1600-1604.

732 Vanselow, A.P., 1932. Equilibria of the base-exchange reactions of bentonites, permutites,
733 soil colloids, and zeolites. *Soil Science* 33, 95-114.

734 Vidal, O., Dubacq, B., 2009. Thermodynamic modelling of clay dehydration, stability and
735 compositional evolution with temperature, pressure and H₂O activity. *Geochimica et*
736 *Cosmochimica Acta* 73, 6544-6564.

737 Vieillard, P., Blanc, P., Fialips, C.I., Gailhanou, H., Gaboreau, S., 2011. Hydration
738 thermodynamics of the SWy-1 montmorillonite saturated with alkali and alkaline-earth
739 cations: A predictive model. *Geochimica et Cosmochimica Acta* 75, 5664-5685.

740 Vieillard, P., Gailhanou, H., Lassin, A., Blanc, P., Bloch, E., Gaboreau, S., Fialips, C.I., Madé,
741 B., 2019. A predictive model of thermodynamic entities of hydration for smectites:
742 Application to the formation properties of smectites. *Applied Geochemistry* 110,
743 104423.

744 Vinci, D., Dazas, B., Ferrage, E., Lanson, M., Magnin, V., Findling, N., Lanson, B., 2020.
745 Influence of layer charge on hydration properties of synthetic octahedrally-charged Na-
746 saturated trioctahedral swelling phyllosilicates. *Applied Clay Science* 184, 105404.

747 Whittaker, M.L., Lammers, L.N., Carrero, S., Gilbert, B., Banfield, J.F., 2019. Ion exchange
748 selectivity in clay is controlled by nanoscale chemical–mechanical coupling.
749 *Proceedings of the National Academy of Sciences* 116, 22052-22057.

750 Woodruff, W.F., Revil, A., 2011. CEC-normalized clay-water sorption isotherm. *Water*
751 *Resources Research* 47.

